Asymmetric Localization of Light by Second-Harmonic Generation

Hamed Ghaemi-Dizicheh,[1] Amir Targholizadeh,[1] Baofeng Feng,[2] and Hamidreza Ramezani[1,*]

[1] *Department of Physics and Astronomy, University of Texas Rio Grande Valley, Edinburg, Texas 78539, USA*

[2] *School of Mathematical and Statistical Sciences, University of Texas Rio Grande Valley, Edinburg, Texas 78539, USA*

(Received 25 October 2021; revised 11 February 2022; accepted 5 May 2022; published 11 July 2022)

We introduce a nonlinear photonic system that enables asymmetric localization and unidirectional transfer of an electromagnetic wave through the second-harmonic generation process. Our proposed scattering setup consists of a noncentrosymmetric nonlinear slab with nonlinear susceptibility $\chi^{(2)}$ placed to the left side of a one-dimensional periodic linear photonic crystal with an embedded defect. We engineered the linear lattice to allow the localization of a selected frequency $2\omega_\star$ while frequency $\omega_\star$ is in the gap. Thus in our proposed scattering setup, a left-incident coherent transverse electric wave with frequency $\omega_\star$ partially converts to frequency $2\omega_\star$ and becomes localized at the defect layer while the unconverted remaining field with frequency $\omega_\star$ exponentially decays throughout the lattice and gets reflected. For a right-incident wave with frequency $\omega_\star$ there will not be any frequency conversion and the incident wave gets fully reflected. Our proposed structure will find application in designing optical components such as optical sensors, switches, transistors, and logic elements.

DOI: 10.1103/PhysRevApplied.18.014023

I. INTRODUCTION

The method of generating a localized mode in periodic structures has paved its footprints in some photonics systems. One can achieve this localization by breaking the translation symmetry through embedding a defect in a periodic lattice [1–6]. Photonic crystal lasers [7–9], strain field traps [10], strong photon localization [11], and mode selection [12] are instances for applications of defect mode in periodic photonic systems.

Because of the time-reversal symmetry, the photon confinement happens regardless of the direction of the incident electromagnetic wave. In recent years, the applications of asymmetric transport have drawn attention in optical systems [13–21], acoustics [22–28], and electronics [29,30]. To create a system with nonreciprocal light-propagation characteristics, we can apply some techniques such as magnetic biasing [31–33], and spatiotemporally modulating index of refraction [34]. In the last method, the frequency and wavevector of the photon shift simultaneously during the photonic transition process. One can embed a defect in spatiotemporally periodic modulated photonic lattice to localize photons in a nonreciprocal manner [35]. While spatiotemporal modulation is a powerful method to attain unidirectional localization, deriving the system and achieving such modulation in practice, specifically in a high-frequency regime, is arduous. This is due to the fact that at higher frequencies one needs to change the medium physical properties, for instance, index of refraction, at the speed that the photons are traveling in the medium. Achieving such fast modulation is not a trivial task. Consequently, it is imperative to propose a photonic structure capable of localizing photons asymmetrically such that it does not need modulation during photon transmission.

This paper provides a technique of asymmetric photon localization by exploiting second-harmonic generation (SHG). The process of SHG is the well-known observation in nonlinear optics where an electromagnetic wave, called a fundamental wave (FW), interacts with the nonlinear material and generates an alternative wave with twice the frequency of initial light. The generated wave is referred to as the second-harmonic wave (SHW). To achieve the asymmetric localization, we introduce an optical setup consisting of a nonlinear slab located to the left side of a linear periodic lattice. By embedding an engineered defect in the linear lattice, we show that the generated SHW becomes localized with a finite transmission while the remaining unconverted FW gets reflected by the band gap. In the opposite direction, the photon in the same frequency as the fundamental wave gets totally reflected.

We employ the transfer matrix approach to study our scattering system. This approach provides us with a theoretical understanding of the idea investigated in this paper for asymmetric localization. The transfer matrix approach for a second-harmonic generation as a method has been developed in optical systems to address low nonlinear

*hamidreza.ramezani@utrgv.edu

conversion efficiency [36–38]. We apply a similar approach in a different context to deal with our scattering problem. Indeed, we extend a formalism that is introduced in Refs. [39,40] for a nonlinear scattering process by combining it with the scattering formalism for linear layered medium. The main characteristic of the transfer matrix for nonlinear scattering potential is that its entries depend on the amplitudes of incoming waves. This property in some nonlinear scattering problems makes it complicated to find the nonlinear transfer matrix. However, despite its severity, the main motivation for using a nonlinear transfer matrix is its composition rule.

Throughout the process of generating a second harmonic, the fundamental and generated electromagnetic fields satisfy a system of nonlinear coupled Helmholtz equations [41]. The solution of these equations in a slowly varying envelope approximation is given in terms of the Jacobi elliptic functions. Instead of implementing these special functions in our analytical calculations, we consider a simplified approach to describing the solution associated with generated second harmonic more straightforward, allowing us to be more focused on the physics behind the observed phenomenon. In this approach, we suppose that the energy conversion to the second harmonic is very low such that the fundamental wave remains essentially undepleted. This process is known as a nondepletion approximation in SHG [42]. To show that our approximation method gives a qualitatively correct result in the last section, we use the finite-element method to demonstrate asymmetric photon localization in a system with similar composition.

II. SCATTERING SETUP

To facilitate the semianalytical approach, let us consider a photonic scattering setup as depicted in Fig. 1(a) including a nonlinear material with nonlinear susceptibility $\chi^{(2)}$ located to the left side of a one-dimensional photonic crystal structure $\mathcal{S}_L$ with a distance δ. The linear lattice is made of N segments of length d, and each segment consists of two homogeneous slabs. The thickness and the refractive index of slab I are, respectively, d_1 and $n_1(\omega)$, while those for slab II are d_2 and $n_2(\omega)$, then we have $d = d_1 + d_2$. Here we consider that, in general, a medium's refractive index depends on the frequency (ω) of passing light. We can embed a defect by breaking the translation symmetry in the periodic linear lattice. To do this, we manipulate segment N_j by changing one of its slab's thickness or substituting it with dissimilar material whose refractive index is different from the other part of the lattice.

In Fig. 1(a), the gray rectangle is demonstrating the nonlinear slab that generates the SHW. On the right side, we show the defect layer of the linear periodic structure with green color in which d_3 and $n_3(\omega)$ stand for its thickness and refractive index, respectively.

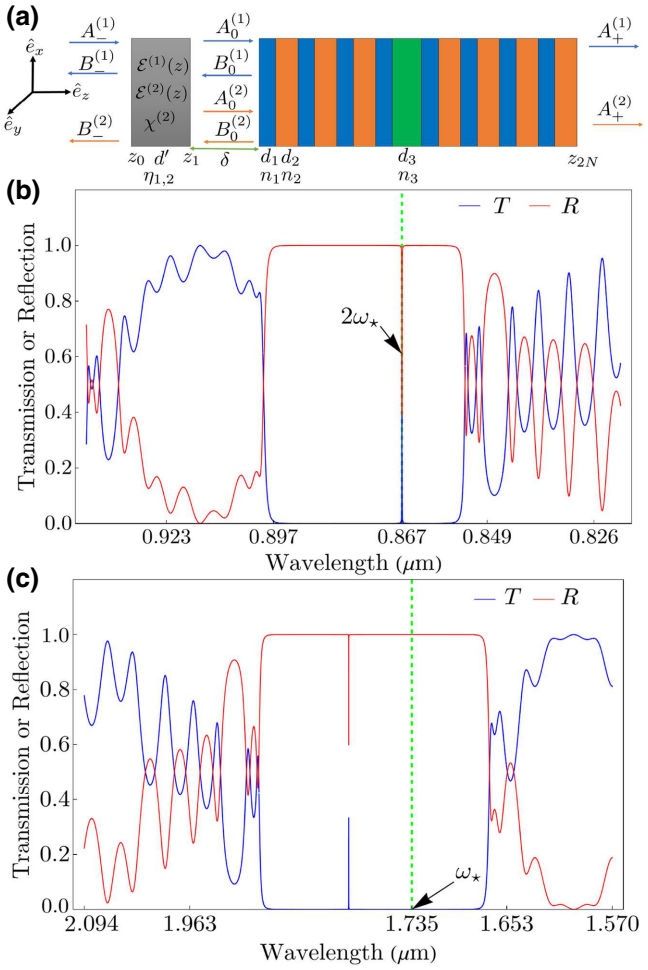

FIG. 1. (a) Schematic diagram of scattering setup consists of a nonlinear material (gray) $\mathcal{S}_N$ and one-dimensional defective photonic crystal $\mathcal{S}_L$. The defect is depicted in green. In this diagram, to embed a defect layer, the linear lattice consists of eight segments in which the second slab of segment four is manipulated. (b),(c) Transmission $T := |t|^2$ and reflection $R := |r|^2$ spectrum of the defective linear photonic crystal in the ranges of $\lambda = 0.924 - 0.821$ μm and $\lambda = 2.094 - 1.570$ μm. The arrows indicate the transmission amplitude for the FW (with frequency $\omega_\star$) and SHW (with frequency $2\omega_\star$).

Consider a normally left incident electromagnetic wave with frequency $\omega = \omega_1$ hits the system in which its electric field is given by

$$\vec{E}(\vec{r}, t) = \mathcal{E}(z)E_x(x)e^{-i\omega_1 t}\hat{e}_y, \tag{1}$$

where $E_x(x)$ is a component of the electric field along the x direction and has the form of $e^{ik_x x}$, with k_x as the wave number along the x direction, $\mathcal{E}(z)$ is the complex amplitude of the electric field, and $\hat{e}_y$ is the unit vector pointing along the y axis. The propagation of the fundamental wave in the nonlinear slab $\mathcal{S}_N$ excites the second nonlinear polarization $\mathbf{P}_{NL} = \epsilon_0 \chi^{(2)} \vec{E} \cdot \vec{E}$. The induced polarization by the nonlinear medium acts as a source and creates

the second-harmonic field with frequency $\omega_2 := 2\omega_1$. The whole nonlinear process can be described by the following nonlinear couple equation [41]:

$$\mathcal{E}^{(1)''} + \eta_1^2 k_1^2 \mathcal{E}^{(1)} = -k_1^2 \chi^{(2)} \mathcal{E}^{(1)*} \mathcal{E}^{(2)}, \tag{2}$$

$$\mathcal{E}^{(2)''} + \eta_2^2 k_2^2 \mathcal{E}^{(2)} = -k_2^2 \chi^{(2)} (\mathcal{E}^{(1)})^2. \tag{3}$$

Here, $k_1 := \omega_1/c$ is the wave number, c is the speed of light in vacuum, $k_2 := \omega_2/c$ is the wave number of the SHW and $\eta_1 := n(\omega_1)$ and $\eta_2 := n(\omega_2)$ are, respectively, the refractive index of the nonlinear medium for the fundamental $\mathcal{E}^{(1)}$ and second-harmonic wave $\mathcal{E}^{(2)}$. In the case of the undepleted fundamental wave, the right side of Eq. (2) becomes infinitesimal in comparison with the left side, and we can neglect it. Then Eq. (2) admits the following linear solution:

$$\mathcal{E}^{(1)}(z) = C^{(1)} e^{ik_1\eta_1 z} + D^{(1)} e^{-ik_1\eta_1 z}. \tag{4}$$

Here, $C^{(1)}$ and $D^{(1)}$ are the complex-valued plane-wave coefficients of FW and, respectively, denote forward and backward propagating waves. Then by substituting $\mathcal{E}^{(1)}$ from the above equation into Eq. (3), we get a nonhomogeneous wave equation such that the right-hand side acts as a source for the SHW induced by FW through the second-order coefficient $\chi^{(2)}$ of the nonlinear medium. Through this process we can express the solution of Eq. (3) as

$$\begin{aligned}\mathcal{E}^{(2)}(z) = {} & C^{(2)} e^{ik_2\eta_2 z} + D^{(2)} e^{-ik_2\eta_2 z} \\ & + \chi^{(2)} \mathcal{G}_1 [(C^{(1)})^2 e^{2ik_1\eta_1 z} + (D^{(1)})^2 e^{-2ik_1\eta_1 z}] \\ & + \chi^{(2)} \mathcal{G}_2 C^{(1)} D^{(1)},\end{aligned} \tag{5}$$

where $\mathcal{G}_1 := -k_2^2/(k_2^2\eta_2^2 - 4k_1^2\eta_1^2)$, $\mathcal{G}_2 := -1/\eta_2^2$ and, similar to the pumping wave, $C^{(2)}$ and $D^{(2)}$ are the complex-valued plane wave coefficients of SHW.

By adding a photonic crystal on the right side of nonlinear slab $\mathcal{S}_N$, we construct a scattering setup for both fundamental and second-harmonic waves. In other words, we wish to construct a scattering solution in the form

$$\mathcal{E}^{(l)}(z) := \begin{cases} A_-^{(l)} e^{ik_{1,2}z} + B_-^{(l)} e^{-ik_{1,2}z} & z < z_0, \\ \mathcal{E}^{(l)}(z) & z \in [z_0, z_1], \\ A_j^{(l)} e^{ik_{1,2}\eta_j z} + B_j^{(l)} e^{-ik_{1,2}\eta_j z} & z \in [z_j, z_{j+1}], \\ A_+^{(1,2)} e^{ik_{1,2}z} & z > z_{2N}, \end{cases} \tag{6}$$

where $l = 1$ ($l = 2$) stands for fundamental (second-harmonic) wave and, $j := 1, \ldots, 2N-1$ labels slabs in the linear multilayered slab $\mathcal{S}_L$.

We aim to show that for an incident wave with specific frequency $\omega_1 := \omega_\star$, our scattering system transfers the generated wave with frequency $2\omega_\star$ and bans the incident fundamental wave from the left, i.e., $A_+^{(1)} = 0$. For the right incoming wave, our system completely acts as a mirror and fully reflects the fundamental wave with frequency $\omega_\star$.

We theoretically analyze our system by applying the transfer matrix approach. In this approach, we consider the scattering process of the left and right incident wave in the following steps:

a. The fundamental wave propagating in the nonlinear medium induces the nonlinear polarization in which it radiates SHW. In general and without considering nondepletion fundamental wave, the propagation of the initial fundamental wave and the second-harmonic wave can be characterized by the nonlinear transfer matrix $\mathbf{M}_N^{(1,2)}$. The entries of the nonlinear transfer matrix for both FW and SHW can be given in terms of the solutions of Eqs. (2) and (3) for $\mathcal{E}^{(1,2)}$. The main characteristic of the nonlinear transfer matrix is that its entries depend on the incident amplitudes $A_-^{(1,2)}$ and $B_-^{(1,2)}$ and they are not unique [40]. However in the nondepletion regime, the nonlinear transfer matrix for the fundamental wave reduces to the linear one.

b. The FW and SHW created inside the nonlinear medium propagate through the linear periodic structure. The scattering of both waves can be given by the linear transfer matrix $\mathbf{M}_L(\omega)$. The combination of these two steps can be expressed by a single transfer matrix given by

$$\mathbf{M}^{(1,2)} = \mathbf{M}_L(\omega_{1,2}) \cdot \mathbf{M}_N^{(1,2)}. \tag{7}$$

In particular, for $n_0 = 1$, the linear transfer matrix $\mathbf{M}_L$ is uniquely determined by the reflection and transmission amplitudes of the linear crystal $\mathcal{S}_L$. They are given by the following relation [43]:

$$\begin{aligned} [\mathbf{M}_L]_{11} &= t - \frac{r_l r_r}{t}, \quad [\mathbf{M}_L]_{12} = \frac{r_r}{t}, \\ [\mathbf{M}_L]_{21} &= -\frac{r_l}{t}, \quad [\mathbf{M}_L]_{12} = \frac{1}{t}, \end{aligned} \tag{8}$$

where $t := t(\omega)$ is the transmission amplitude, and $r_l := r_l(\omega)$ ($r_r := r_r(\omega)$) is left (right) reflection amplitude. According to Eqs. (7) and (8) and in light of the scattering solution (6), the scattering of the generated wave is given by the following relation:

$$\begin{aligned} \begin{pmatrix} A_+^{(2)} \\ 0 \end{pmatrix} &= \mathbf{M}^{(2)} \begin{pmatrix} A_-^{(2)} \\ B_-^{(2)} \end{pmatrix} = \mathbf{M}_L(\omega_2) \cdot \mathbf{M}_N^{(2)} \begin{pmatrix} A_-^{(2)} \\ B_-^{(2)} \end{pmatrix} \\ &= \mathbf{M}_L(\omega_2) \begin{pmatrix} A_0^{(2)} \\ B_0^{(2)} \end{pmatrix} = \frac{1}{t} \begin{pmatrix} [t^2 - r_l r_r] A_0^{(2)} + r_r B_0^{(2)} \\ -r_l A_0^{(2)} + B_0^{(2)} \end{pmatrix}. \end{aligned} \tag{9}$$

This in turns implies

$$B_0^{(2)} - r_l(2\omega) A_0^{(2)} = 0, \quad A_+^{(2)} = t(2\omega) A_0^{(2)}. \tag{10}$$

Following the similar steps for the FW we have

$$B_0^{(1)} - r_l(\omega)A_0^{(1)} = 0, \quad A_+^{(1)} = t(\omega)A_0^{(1)}. \tag{11}$$

In the above equation, the intermediate amplitudes $A_0^{(1,2)}$ and $B_0^{(1,2)}$ are complex-valued functions of incident amplitudes. Equations (10) and (11) form a system of complex-valued equations where one can solve it to get the scattering amplitudes $B_-^{(1,2)}$ and $A_+^{(1,2)}$.

For the right-incident wave, the scattering solution is given by Eq. (6) for $z \in (z_0, z_{2N})$ and for elsewhere, we have

$$\mathcal{E}(z) := \begin{cases} B_-^{(1,2)} e^{-ik_{1,2}z}, & z < z_0, \\ A_+^{(1,2)} e^{ik_{1,2}z} + B_+^{(1,2)} e^{-ik_{1,2}z} & z > z_{2N}, \end{cases} \tag{12}$$

The scattering amplitudes of the system for the right-incoming wave can be given by the following transfer matrix:

$$\mathbf{M}^{(1,2)} = \mathbf{M}_N^{(1,2)} \cdot \mathbf{M}_L^{-1}, \tag{13}$$

where $\mathbf{M}_L^{-1}$ is the inverse of the linear transfer matrix and $\mathbf{M}_N^{(1,2)}$ is the nonlinear transfer matrix that its entries depends on $A_+^{(1,2)}$ and $B_+^{(1,2)}$. By applying the above transfer matrix, we find

$$B_-^{(j)} = \frac{\det \mathbf{M}_N^{(j)}}{[\mathbf{M}_N^{(j)}]_{11}} B_0^{(j)}, \quad A_0^{(j)} = -\frac{[\mathbf{M}_N^{(j)}]_{12}}{[\mathbf{M}_N^{(j)}]_{11}} B_0^{(j)}, \tag{14}$$

where $j = 1, 2$ and

$$B_0^{(j)} = \frac{r_l(\omega_j)}{t(\omega_j)} A_+^{(j)} + [t(\omega_j) - \frac{r_l(\omega_j) r_r(\omega_j)}{t(\omega_j)}] B_+^{(j)}, \tag{15}$$

$$A_0^{(j)} = \frac{1}{t(\omega_j)} A_+^{(j)} - \frac{r_l(\omega_j)}{t(\omega_j)} B_+^{(j)}. \tag{16}$$

In general, the entries of the nonlinear transfer matrix $\mathbf{M}_N$ can be given in terms of the exact solutions of Eqs. (2) and (3) [41]. In light of them, the system of Eqs. (10) and (11) consists of Jacobi elliptic functions where scattering amplitudes appear in the elliptic integral of the first kind. Therefore, finding the analytic scattering solution of the second-harmonic generation is possible but complicated.

Under the nondepletion limit, the second-harmonic generation admits a manageable solution, Eq. (5), which makes it feasible to find the entries of the nonlinear transfer matrix. Given the nondepletion regime, the nonlinear transfer matrix of the fundamental wave $\mathbf{M}_N^{(1)}$ reduces to the linear one. In the Appendix, we introduce the nonlinear transfer matrix for the SHW that illuminates the system from the left. Here, we suppose that there is no left incident wave with the same frequency as the second harmonic, i.e., $A_-^{(2)} = 0$ and the second-harmonic reflection emerges through the reflection from the surfaces.

Our strategy for localizing the SHW is to engineer the band structure of the linear lattice $\mathcal{S}_L$ by embedding defects in the linear crystal. This manufacturing can be done by tuning the thickness of layers, and refractive indices of the linear crystal. Those parameters, as mentioned here, indeed provide the degrees of freedom in our system to apply optimization and reach a desirable band structure of the system. In our system, we implement this optimization to get the wave number $k_\star := \omega_\star/c$ for the fundamental wave lies in the stopband, and simultaneously, the wave number $2k_\star$ for the SHW stands on the passband.

Allowing that, on the right hand of Eq. (10), the transmission coefficient for the SHW, i.e., $t^{(2)}(2k_\star)$ takes a finite value while for the FW, it vanishes. Subsequently, it can be seen easily from Eqs. (10) and (11) for the $\omega = \omega_\star$, that the transmitted amplitudes satisfy the following relations [44]:

$$A_+^{(1)} = 0, \quad A_+^{(2)} \notin 0. \tag{17}$$

This solution leads to a localized SHW with frequency $2\omega_\star$ in the defect layer of the linear system and exponentially decayed FW [45]. The wave number lies in the stopband for the right incident wave with frequency $\omega_\star$, which means the transmission coefficient is zero. By substituting $t(\omega_\star)$ in Eqs. (15) and (16), we have

$$A_0^{(1)} = B_0^{(1)} = 0. \tag{18}$$

In this case, the photonic crystal totally reflects the wave, and there is no passing FW in the nonlinear medium. In other words, the source term generating a second harmonic is absent. Consequently, the right incident fundamental wave exponentially decays in the linear lattice.

In Figs. 1(b) and 1(c), we plot the transmission and reflection for the linear multilayered structure with a defect layer. In our design, the defective linear crystal consists of $N = 8$ segments each made of two slabs with refractive index $n_1 = 1.2$ (blue layer) and $n_2 = 3.2$ (orange layer) and slabs take the same thickness, i.e., $d_1 = d_2 = 1$ μm. The linear structure becomes defective by making twice the thickness of the second slab of the fourth segment ($d_3 = 2$ μm).

The transmission coefficient $T := |t|^2$ and reflection coefficient $R := |r|^2$ are given by Eq. (8). We plot them in terms of the wavelength in Figs. 1(b) and 1(c). One can see that defect state appears within the photonic band gap between 0.924–0.821 μm (left diagram) and 2.094–1.570 μm (right diagram). For this defective structure, a fundamental wave with $\omega_\star = 10.783 \times 10^2$ Hz is trapped through the crystal while the generated wave with frequency $2\omega_\star$ is transmitted. In Fig. 2, we plot the intensity of the transmitted fundamental and second-harmonic

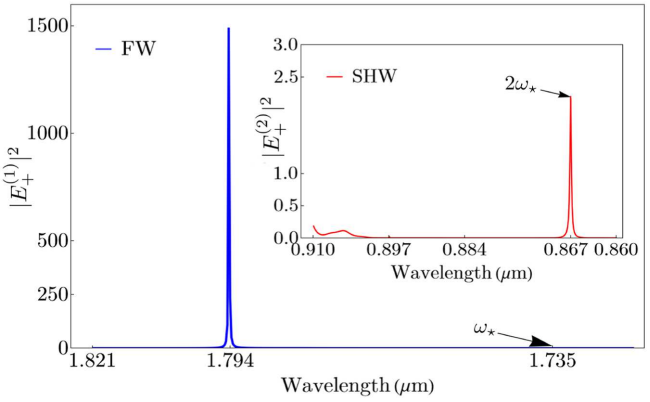

FIG. 2. Transmitted intensity $|E_+^{(1,2)}|^2 = |A_+^{(1,2)}|^2$ of the FW (blue line) and SHW (red line) for the left incident wave. The arrows indicate the value of transmitted intensity at $\lambda_\star$ and $2\lambda_\star$.

wave $|E_+^{(1)}|^2 = |A_+^{(1)}|^2$ ($|E_+^{(2)}|^2 = |A_+^{(2)}|^2$) for the left incident wave. In this diagram, $|E_+^{(1)}(\omega_\star)|^2/|E_+^{(2)}(2\omega_\star)|^2 \approx 10^{-2}$. In the calculation, the second-order nonlinear coefficient for the nonlinear slab is $\chi^{(2)} = 100$ pm/V and the refractive index for the FW and SHW is, respectively, $\eta_1 = 3.21$ and $\eta_2 = 3.22$. Since the efficiency of the nonlinear medium is very low, we assume that a strong light with an amplitude $|E_0| = |A_-| = 100V/\mu$m incident normally on the system. In this case the localization and the transmission of the passing SHW is detectable. A large value of nonlinear susceptibility taken in our data does not exclude the practical application for our proposed setup since, first, we use the approximation to solve the nonlinear differential equations associated with our system and, second, there are studies showing the possibility of creating large optical nonlinearity in photonic systems [46,47]. The intensity distribution of the FW and SHW into the linear defective crystal is plotted in Fig. 3. For the left incident wave, the SHW localizes through the defective layer while the FW exponentially decays. We also show the mode distribution of the right coming wave. One can see that the FW exponentially decays in the linear lattice.

III. NUMERIC SIMULATION

This section numerically demonstrates second-harmonic localization by using the finite-element-method simulations in a time-dependent area. We use COMSOL Multiphysics to perform a time-domain transient simulation of a sinusoidal wave passing through an optical setup, which is similar to the one we depict in Fig. 1(a). In our codes, we consider that our linear crystal consists of 12 segments made of two slabs with refractive index $n_1 = 1.2$ and $n_2 = 3.2$. Our linear system has been made defective by adding an extra slab in the middle of the crystal. The optimization of the linear system for finding an appropriate band gap in the way that the generated frequency stands on

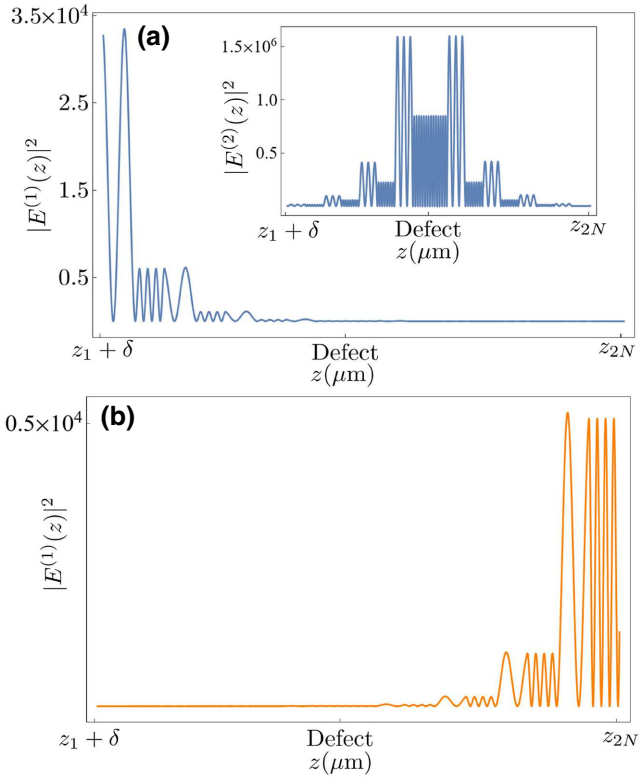

FIG. 3. (a) Intensity distribution of the left incident FW and SHW (inset), and (b) the right incident FW into linear photonic crystal at $\lambda_\star = 1.736$ μm.

the passing band determines the length of slabs and defect layer. The optimization defines the length of slabs such that $d_1 = 0.2$ μm, $d_2 = 0.26$ μm, and $d_3 = 1.593$ μm. Figure 4 illustrates the corresponding transmission and reflection amplitudes of the linear crystal in the logarithmic scale. Regarding these plots, one can see that the asymmetric localization takes place for the left incoming photon with frequency $\omega_\star = 282.82$ Hz. The nonlinearity is enrolled in our simulation by considering the coupling between fundamental wave and second-harmonic wave via the following polarization:

$$\mathbf{P}_{NL}^{(1)} = 2d_{\text{eff}}E^{(2)}E^{(1)*}, \quad \mathbf{P}_{NL}^{(2)} = d_{\text{eff}}(E^{(1)})^2, \qquad (19)$$

where we aligned our polarization in y-direction and d_{eff} is nonlinear coefficient for the SHG process. We then probe the transient on the right side of our system and measure the amplitude of time dependent electric field. The corresponding contribution of an electric field for different modes in the frequency domain is given by the Fourier transformation.

In Fig. 5, we show the mode contribution of the FW at $\omega_\star = 282.82$ THz and SHW at $2\omega_\star = 565.65$ THz. The density of the electromagnetic wave in the linear photonic crystal is depicted in Fig. 6(a) showing that the FW is exponentially decayed in the defective linear system while the

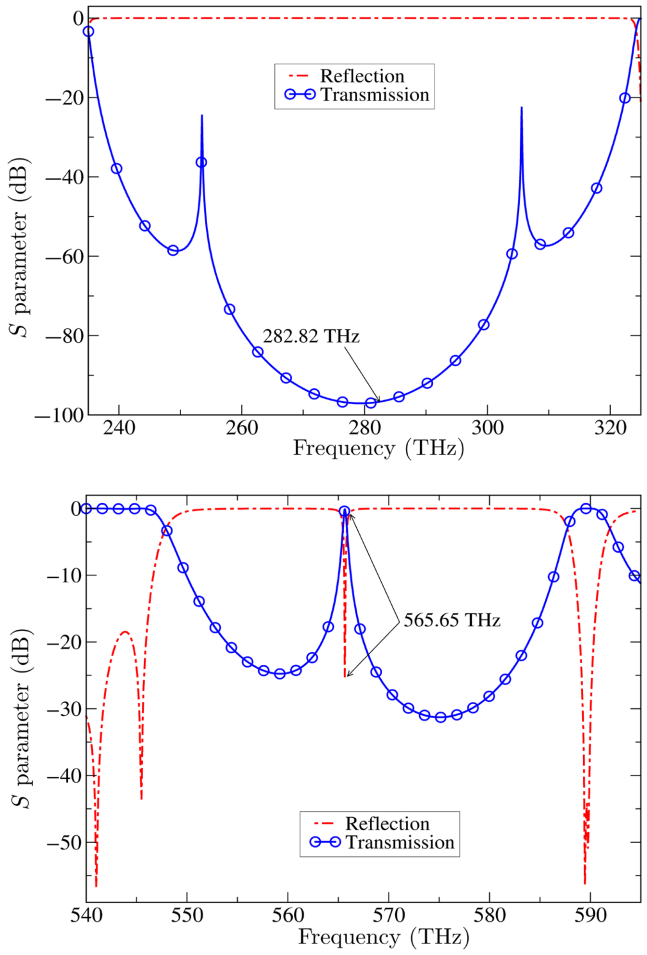

FIG. 4. Logarithmic diagram of transmission $T := |t|^2$ and reflection $R := |r|^2$ spectrum of the defective linear photonic crystal in the numeric simulation. In the upper diagram, the frequency of the fundamental wave ($\omega_\star = 282.82$ THz) lies in the band gap while the second harmonic generated frequency $2\omega_\star$ is located on the passband.

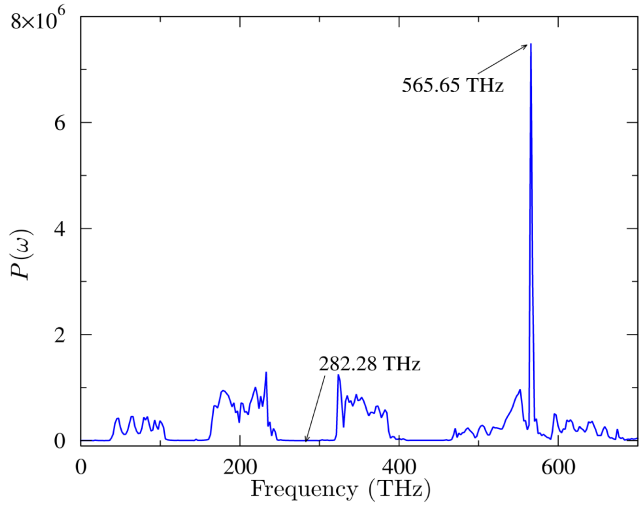

FIG. 5. This plot shows the contribution of the transmitted wave ($P(\omega) := |\mathfrak{a}(\omega)|^2$) versus frequency derived from the Fourier transform of the time domain transient. Here $\mathfrak{a}(\omega)$ is the electric field mode in frequency domain. The first and second marked point represents $P(\omega_\star)$ and $P(2\omega_\star)$ for the fundamental and the second harmonic.

SHW is localized in the defect layer. For the right incident wave with the frequency $\omega_\star$, we find the mode intensity in Fig. 6(b) and show that the FW exponentially decays in the photonic crystal.

In summary, we suggest an optical system that makes the photon localized when it hits the photonic system from one particular side. In our method for asymmetric localization, the incident wave is reflected from the optical device while the generated harmonic wave transfers. The system is adjustable in which one can manipulate the linear crystal and its defect to localize higher generated harmonic. We employ two distinct approaches based on nondepletion approximation and finite-element method to demonstrate such asymmetric localization. We apply the nonlinear transfer matrix to find the scattering solutions in the former one. The nonlinear transfer-matrix method can be extended beyond the nondepletion approximation by the considering exact solution of the nonlinear equation. Also, the result based on the nondepletion limit can be optimized by a technique of shooting method [48]. Our proposed photonic structure can be employed in designing optical sensors [49] and unidirectional lasers [50]. Moreover, the unidirectional characteristic of our system for localizing photons makes it potentially a candidate for designing optical devices, which is cutting-edge research nowadays, precisely because of their application in optical communication and signal processing. While we consider a lossless photonic structure in our approach for localizing photons, this method can be extended to the more practical one where losses appear from the strong light-matter interaction. In the case of a lossy system, one can explore the implementation of light-stopping techniques [51,52] to improve the system's effectiveness under experimental conditions. In the case of high-efficiency harmonic generation where the fundamental mode almost totally transforms to higher harmonics, one can simply make changes in the linear part of our setup to have asymmetric localization of fundamental wave.

To sum up, unidirectional localizing by generating higher harmonic and tuning the localized frequency by engineering the band structure of the periodic layer are the most important outcomes of this paper, making it an alternative in the field of light localization. An interesting future extension of this work could be in the generation of asymmetric qubits for quantum applications using defect centers.

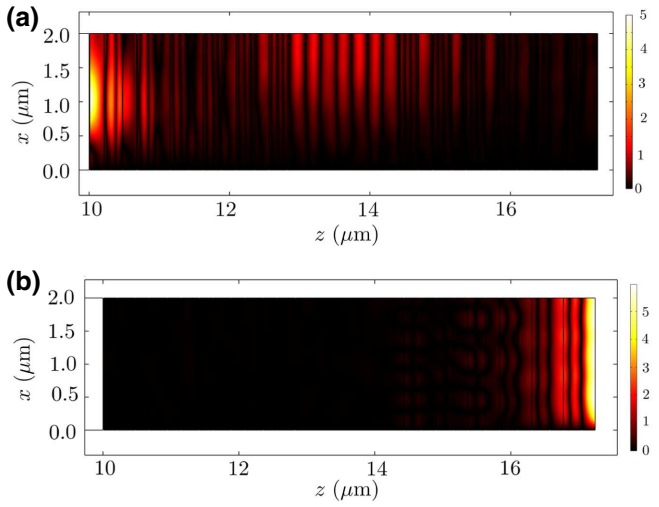

FIG. 6. In these figures, we demonstrate the mode density throughout the linear crystal. For the left incident wave (a), the higher intensity on the left side corresponds to the fundamental wave. One can see the localized SHW in the middle of the diagram in the defect layer. For the right incident wave (b), the higher intensity on the right side corresponds to the exponentially decaying fundamental wave. In the diagram, the vertical axis represents the spatial extension of the linear part in x direction while the horizontal axes represents the size in z direction. The color bar demonstrates the norm of electric field ($10^4 \times$ V/m).

ACKNOWLEDGMENTS

H.R. acknowledges the support by the Army Research Office Grant No. W911NF-20-1-0276 and NSF Grant No. PHY-2012172. The views and conclusions contained in this document are those of the authors and should not be interpreted as representing the official policies, either expressed or implied, of the Army Research Office or the U.S. Government. The U.S. Government is authorized to reproduce and distribute reprints for Government purposes notwithstanding any copyright notation herein.

APPENDIX: NONLINEAR TRANSFER MATRIX

In this Appendix, we construct the nonlinear transfer matrix of a nonlinear layer under the nondepletion signal approximation [36,38]. In terms of the definition of transfer matrix [43] and continuity condition for electric field $\vec{E}$ and magnetic field $\vec{H}$ at $z = z_0, z_1$ [53], the transfer matrix $\mathbf{M}_2$ of slab $\mathcal{S}_1$ for second-harmonic generation can be given by the following relation:

$$\begin{pmatrix} A_0^{(2)} \\ B_0^{(2)} \end{pmatrix} = \mathcal{M}_L^{(2)} \begin{pmatrix} 0 \\ B_-^{(2)} \end{pmatrix} + \chi^{(2)} \mathcal{M}_N^{(2)}(A_-^{(1)}, B_-^{(1)}) \begin{pmatrix} A_-^{(1)} \\ B_-^{(1)} \end{pmatrix}. \tag{A1}$$

The first term on the right side presents the linear transfer matrix, which is generated by the homogenous solution of Eq. (3) of the main text and relates the free-wave amplitude of the second harmonic field on both sides of the nonlinear medium. It is given by the following relation:

$$\mathcal{M}_L^{(2)} = \frac{1}{\eta_2} \mathbf{Q}_{-1}^{(2)} \mathbf{K}_+^{(2)} \mathbf{P}_{+1}^{(2)} \mathbf{P}_{-0}^{(2)} \mathbf{K}_-^{(2)} \mathbf{Q}_{+0}^{(2)}. \tag{A2}$$

The related matrices are defined as

$$\mathbf{Q}_{\pm j}^{(i)} = \begin{pmatrix} e^{\pm i k_i z_j} & 0 \\ 0 & e^{\mp i k_i z_j} \end{pmatrix}, \mathbf{P}_{\pm j}^{(i)} = \begin{pmatrix} e^{\pm i \tilde{k}_i z_j} & 0 \\ 0 & e^{\mp i \tilde{k}_i z_j} \end{pmatrix}, \quad \mathbf{K}_\pm^{(j)} = \frac{1}{2\eta_j} \begin{pmatrix} \eta_j + 1 & \pm\eta_j \mp 1 \\ \pm\eta_j \mp 1 & \eta_j + 1 \end{pmatrix}, \tag{A3}$$

and $\tilde{k}_j = \eta_j k_j$. The second part in Eq. (3) of the main text denotes the nonlinear transfer matrix, which relates the bound-wave amplitudes of the second-harmonic field created by the fundamental wave. We find the nonlinear transfer matrix as

$$\mathcal{M}_N^{(2)} = \frac{\mathcal{G}_1}{2\tilde{k}_2} \mathbf{Q}_{-1}^{(2)} [\mathbf{K}\mathbf{O}_1 - \tilde{\mathbf{K}}\mathbf{O}_0] \mathbf{N}_1 \mathbf{P}_{-0}^{(1)} \mathbf{K}_+^{(1)} \mathbf{Q}_+^{(1)} + \mathcal{G}_2 \mathbf{Q}_{-1}^{(2)} \mathbf{N}_2 \mathbf{P}_{-0}^{(1)} \mathbf{K}_+^{(1)} \mathbf{Q}_+^{(1)}, \tag{A4}$$

where

$$\tilde{\mathbf{K}} = \begin{pmatrix} \tilde{k}_2 + 2\tilde{k}_1 & \tilde{k}_2 - 2\tilde{k}_1 \\ \tilde{k}_2 + 2\tilde{k}_1 & \tilde{k}_2 - 2\tilde{k}_1 \end{pmatrix}, \quad \mathbf{K} = \begin{pmatrix} k_2 + 2\tilde{k}_1 & k_2 - 2\tilde{k}_1 \\ k_2 + 2\tilde{k}_1 & k_2 - 2\tilde{k}_1 \end{pmatrix}, \quad \mathbf{O}_j = \begin{pmatrix} e^{2i\tilde{k}_1 z_j} & 0 \\ 0 & e^{-2i\tilde{k}_2 z_j} \end{pmatrix}, \tag{A5}$$

and, we introduce amplitude-dependant matrices

$$\mathbf{N}_1 = \begin{pmatrix} C^{(1)} & 0 \\ 0 & D^{(1)} \end{pmatrix}, \quad \mathbf{N}_2 = \begin{pmatrix} 0 & C^{(1)} \\ D^{(1)} & 0 \end{pmatrix}. \tag{A6}$$

The amplitudes $C^{(1)}$ and $D^{(1)}$ can be defined from the FW such as

$$\begin{pmatrix} C^{(1)} \\ D^{(1)} \end{pmatrix} = \mathbf{P}_{-0}^{(1)} \mathbf{K}_+^{(1)} \mathbf{Q}_{+0}^{(1)} \begin{pmatrix} A_-^{(1)} \\ B_-^{(1)} \end{pmatrix}. \tag{A7}$$

[1] J. Joannopoulos, R. Meade, and J. Winn, *Photonic Crystals–princeton* (Princeton, NJ, 1995).

[2] S. Noda, A. Chutinan, and M. Imada, Trapping and emission of photons by a single defect in a photonic bandgap structure, Nature **407**, 608 (2000).

[3] Y. Akahane, T. Asano, B.-S. Song, and S. Noda, High-Q photonic nanocavity in a two-dimensional photonic crystal, Nature **425**, 944 (2003).

[4] B.-S. Song, S. Noda, T. Asano, and Y. Akahane, Ultra-high-Q photonic double-heterostructure nanocavity, Nat. Mater. **4**, 207 (2005).

[5] M. Navadeh-Toupchi, F. Jabeen, D. Oberli, and M. Portella-Oberli, Localized Photon Lasing in a Polaritonic Lattice Landscape, Phys. Rev. Appl. **14**, 024055 (2020).

[6] F. Mostafavi, C. Yuce, O. S. Maganã Loaiza, H. Schomerus, and H. Ramezani, Robust localized zero-energy modes from locally embedded $\mathcal{PT}$-symmetric defects, Phys. Rev. Res. **2**, 032057 (2020).

[7] O. Painter, R. K. Lee, A. Scherer, A. Yariv, J. D. O'Brien, P. D. Dapkus, and I. Kim, Two-dimensional photonic bandgap defect mode laser, Science **284**, 1819 (1999).

[8] H.-G. Park, S.-H. Kim, S.-H. Kwon, Y.-G. Ju, J.-K. Yang, J.-H. Baek, S.-B. Kim, and Y.-H. Lee, Electrically driven single-cell photonic crystal laser, Science **305**, 1444 (2004).

[9] B. Ellis, M. A. Mayer, G. Shambat, T. Sarmiento, J. Harris, E. E. Haller, and J. Vučković, Ultralow-threshold electrically pumped quantum-dot photonic-crystal nanocavity laser, Nat. Photonics **5**, 297 (2011).

[10] A. J. Sievers and S. Takeno, Intrinsic Localized Modes in Anharmonic Crystals, Phys. Rev. Lett. **61**, 970 (1988).

[11] S. John, Strong Localization of Photons in Certain Disordered Dielectric Superlattices, Phys. Rev. Lett. **58**, 2486 (1987).

[12] C. Poli, M. Bellec, U. Kuhl, F. Mortessagne, and H. Schomerus, Selective enhancement of topologically induced interface states in a dielectric resonator chain, Nat. Commun. **6**, 1 (2015).

[13] H. Ramezani, T. Kottos, R. El-Ganainy, and D. N. Christodoulides, Unidirectional nonlinear $\mathcal{PT}$-symmetric optical structures, Phys. Rev. A **82**, 043803 (2010).

[14] H. Lira, Z. Yu, S. Fan, and M. Lipson, Electrically Driven Nonreciprocity Induced by Interband Photonic Transition on a Silicon Chip, Phys. Rev. Lett. **109**, 033901 (2012).

[15] D.-W. Wang, H.-T. Zhou, M.-J. Guo, J.-X. Zhang, J. Evers, and S.-Y. Zhu, Optical Diode Made from a Moving Photonic Crystal, Phys. Rev. Lett. **110**, 093901 (2013).

[16] B. Peng, Ş. K. Özdemir, F. Lei, F. Monifi, M. Gianfreda, G. L. Long, S. Fan, F. Nori, C. M. Bender, and L. Yang, Parity–time-symmetric whispering-gallery microcavities, Nat. Phys. **10**, 394 (2014).

[17] J. Fujita, M. Levy, R. Osgood Jr, L. Wilkens, and H. Dötsch, Waveguide optical isolator based on Mach–Zehnder interferometer, Appl. Phys. Lett. **76**, 2158 (2000).

[18] N. Shitrit, J. Kim, D. S. Barth, H. Ramezani, Y. Wang, and X. Zhang, Asymmetric Free-Space Light Transport at Nonlinear Metasurfaces, Phys. Rev. Lett. **121**, 046101 (2018).

[19] F. Nazari, M. Nazari, M. K. Moravvej-Farshi, and H. Ramezani, Asymmetric evolution of interacting solitons in parity time symmetric cells, IEEE J. Quantum Electron. **49**, 932 (2013).

[20] H. Ramezani, Spectral singularities with directional sensitivity, Phys. Rev. A **103**, 043516 (2021).

[21] G.-L. Zhu, A. Targholizadeh, X.-Y. Lu, C. Yuce, and H. Ramezani, Exceptional point generated robust asymmetric high-order harmonics, arXiv preprint arXiv:2201.07663 (2022).

[22] X. Zhu, H. Ramezani, C. Shi, J. Zhu, and X. Zhang, $\mathcal{PT}$-Symmetric Acoustics, Phys. Rev. X **4**, 031042 (2014).

[23] C. Shi, M. Dubois, Y. Chen, L. Cheng, H. Ramezani, Y. Wang, and X. Zhang, Accessing the exceptional points of parity-time symmetric acoustics, Nat. Commun. **7**, 1 (2016).

[24] H. Ramezani, M. Dubois, Y. Wang, Y. R. Shen, and X. Zhang, Directional excitation without breaking reciprocity, New J. Phys. **18**, 095001 (2016).

[25] S. A. Cummer, J. Christensen, and A. Alù, Controlling sound with acoustic metamaterials, Nat. Rev. Mater. **1**, 1 (2016).

[26] R. Fleury, D. L. Sounas, C. F. Sieck, M. R. Haberman, and A. Alù, Sound isolation and giant linear nonreciprocity in a compact acoustic circulator, Science **343**, 516 (2014).

[27] T. Liu, X. Zhu, F. Chen, S. Liang, and J. Zhu, Unidirectional Wave Vector Manipulation in Two-Dimensional Space with an All Passive Acoustic Parity-Time-Symmetric Metamaterials Crystal, Phys. Rev. Lett. **120**, 124502 (2018).

[28] S. Puri, J. Ferdous, A. Shakeri, A. Basiri, M. Dubois, and H. Ramezani, Tunable Non-Hermitian Acoustic Filter, Phys. Rev. Appl. **16**, 014012 (2021).

[29] J. Schindler, Z. Lin, J. Lee, H. Ramezani, F. M. Ellis, and T. Kottos, $\mathcal{PT}$-symmetric electronics, J. Phys. A: Math. Theor. **45**, 444029 (2012).

[30] N. Bender, S. Factor, J. D. Bodyfelt, H. Ramezani, D. N. Christodoulides, F. M. Ellis, and T. Kottos, Observation of Asymmetric Transport in Structures with Active Nonlinearities, Phys. Rev. Lett. **110**, 234101 (2013).

[31] D. Jalas, A. Petrov, M. Eich, W. Freude, S. Fan, Z. Yu, R. Baets, M. Popović, A. Melloni, J. D. Joannopoulos, Mathias Vanwolleghem, Christopher R. Doerr, and Hagen Renner, What is–and what is not–an optical isolator, Nat. Photonics **7**, 579 (2013).

[32] B. E. Saleh and M. C. Teich, *Fundamentals of Photonics* (John Wiley & Sons, Hoboken, 2019).

[33] H. Ramezani, S. Kalish, I. Vitebskiy, and T. Kottos, Unidirectional Lasing Emerging from Frozen Light in Nonreciprocal Cavities, Phys. Rev. Lett. **112**, 043904 (2014).

[34] Z. Yu and S. Fan, Complete optical isolation created by indirect interband photonic transitions, Nat. Photonics **3**, 91 (2009).

[35] H. Ramezani, P. K. Jha, Y. Wang, and X. Zhang, Nonreciprocal Localization of Photons, Phys. Rev. Lett. **120**, 043901 (2018).

[36] J.-J. Li, Z.-Y. Li, and D.-Z. Zhang, Second harmonic generation in one-dimensional nonlinear photonic crystals solved by the transfer matrix method, Phys. Rev. E **75**, 056606 (2007).

[37] M.-L. Ren and Z.-Y. Li, Enhanced nonlinear frequency conversion in defective nonlinear photonic crystals with

designed polarization distribution, J. Opt. Soc. Am. B **27**, 1551 (2010).
[38] H. Li, J. W. Haus, and P. P. Banerjee, Application of transfer matrix method to second-harmonic generation in nonlinear photonic bandgap structures: oblique incidence, J. Opt. Soc. Am. B **32**, 1456 (2015).
[39] A. Mostafazadeh, H. Ghaemi-Dizicheh, and S. Hajizadeh, Blowing up light: A nonlinear amplification scheme for electromagnetic waves, J. Opt. Soc. Am. B **35**, 2986 (2018).
[40] A. Mostafazadeh, Nonlinear scattering and its transfer matrix formulation in one dimension, Eur. Phys. J. Plus **134**, 16 (2019).
[41] R. W. Boyd, *Nonlinear Optics* (Academic press, New York, 2020).
[42] D. Javůrek and J. Peřina, Analytical model of surface second-harmonic generation, Sci. Rep. **9**, 1 (2019).
[43] A. Mostafazadeh, Transfer matrix in scattering theory: A survey of basic properties and recent developments, Turk. J. Phys. **44**, 472 (2020).
[44] For a large number of layers, which is accessible in practice with the current technology, this assumption is valid, and the defect state acts as high-Q cavity for the second-harmonic-generated wave.
[45] A. Figotin and V. Gorentsveig, Localized electromagnetic waves in a layered periodic dielectric medium with a defect, Phys. Rev. B **58**, 180 (1998).
[46] M. Z. Alam, I. D. Leon, and R. W. Boyd, Large optical nonlinearity of indium tin oxide in its epsilon-near-zero region, Science **352**, 795 (2016).
[47] N. Nookala, J. Lee, M. Tymchenko, J. S. Gomez-Diaz, F. Demmerle, G. Boehm, K. Lai, G. Shvets, M.-C. Amann, A. Alu, and M. Belkin, Ultrathin gradient nonlinear metasurface with a giant nonlinear response, Optica **3**, 283 (2016).
[48] J. jer Huang, Q. Feng, X. L. Zhang, and L. Y. Zhang, New transfer-matrix method for frequency conversion in nonlinear multilayered structures based on coupled-amplitude equations, J. Opt. Soc. Am. B **36**, 26 (2019).
[49] J. Haus, *Optical Sensors: Basics and Applications* (John Wiley & Sons, Weinheim, 2010).
[50] H. Ramezani, H.-K. Li, Y. Wang, and X. Zhang, Unidirectional Spectral Singularities, Phys. Rev. Lett. **113**, 263905 (2014).
[51] Extreme control of light in metamaterials: complete and loss-free stopping of light, Physica B: Condensed Matter **407**, 4066 (2012), proceedings of the conference - Wave Propagation: From Electrons to Photonic Crystals and Metamaterials.
[52] K. L. Tsakmakidis, K. Baskourelos, and T. Stefański, Topological, nonreciprocal, and multiresonant slow light beyond the time-bandwidth limit, Appl. Phys. Lett. **119**, 190501 (2021).
[53] J. D. Jackson, Classical electrodynamics (1999).